Geophysical Research Letters

RESEARCH LETTER
10.1029/2020GL089218

Key Points:
- Mg uptake in liquid iron is controlled by the liquid's Si content; silicate Mg is reduced by Si in the metal
- If the core later expelled Mg ingested while accreting as (Mg,Fe)-silicate, it could transfer siderophile trace elements back to the mantle
- ULVZs at the base of the mantle could be related to fractional crystallization of (Mg,Fe) silicate expelled by the core

Supporting Information:
- Supporting Information S1

Correspondence to:
G. Helffrich,
george@elsi.jp

Citation:
Helffrich, G., Hirose, K., & Nomura, R. (2020). Thermodynamical modeling of liquid Fe-Si-Mg-O:molten magnesium silicate release from the core. *Geophysical Research Letters*, *47*, e2020GL089218. https://doi.org/10.1029/2020GL089218

Received 13 JUN 2020
Accepted 1 OCT 2020
Accepted article online 7 OCT 2020

Thermodynamical Modeling of Liquid Fe-Si-Mg-O:Molten Magnesium Silicate Release From the Core

George Helffrich[1], Kei Hirose[1,2], and Ryuichi Nomura[1,3]

[1]Earth-Life Science Institute, Tokyo Institute of Technology, Tokyo, Japan, [2]Department of Earth and Planetary Science, University of Tokyo, Tokyo, Japan, [3]Now at Hakubi Center/Graduate School of Human and Environmental Studies, Kyoto University, Kyoto, Japan

Abstract We developed a thermodynamic model to explore the joint solubility of Mg, Si, and O in liquid Fe on the basis of high-pressure metal-silicate partitioning data in the literature, with more Mg kept in the metal when Si and O are present. With $<1.7 \pm 0.5$ wt% Mg, the metal in the young Earth's core retains Mg as the core evolves and crystallizes SiO_2. Higher Mg concentrations require either the late addition of metal that equilibrated with silicate in a super-liquidus magma ocean or the assimilation of silicate into the core at the time of a giant impact. Above 1.7 wt% Mg, (Mg,Fe)-silicate melts also exsolve from the core and transfer core-hosted elements to the mantle. Fractional crystallization of the core-derived silicate melts in the core or at the core-mantle boundary could, additionally, yield a persistent molten silicate layer that could also contribute to ultralow velocity zone formation in the lowermost mantle.

Plain Language Summary Some think that crystallization of oxide in the liquid core, either MgO or SiO_2, could have been responsible for driving core convection and geodynamo since early Earth times, at least until iron started crystallizing the inner core. However, the joint solubility of Mg, Si, and O in liquid Fe has not been explored yet. Here we developed a thermodynamic model to examine the exsolution of MgO and SiO_2 from liquid Fe at core-mantle boundary (CMB) pressure based on earlier experimental data on metal-silicate partitioning. Our main findings are that (1) more Mg is retained in the presence of Si and O in metal; (2) with <1.7 wt% Mg, the core expels solid SiO_2 but not MgO; and (3) with higher Mg, magnesium silicate melt also exolves and transfers core-hosted elements to the mantle. The seismologically observed molten silicate layer above the CMB may have been originally derived from the core.

1. Introduction

As the Earth accreted, a magma ocean formed in which metal separated from silicate at moderately high pressures, forming the core by a stochastically continuous process (Rubie et al., 2015; Wade & Wood, 2005). The high-temperature metal incorporated small but finite amounts of the lithophile elements Mg, Si, and O that exerted a much larger effect on planetary evolution than their small proportions would suggest.

Recently, both theory (de Koker et al., 2012; Pozzo et al., 2013) and experiments (Gomi et al., 2013; Ohta et al., 2016; Seagle et al., 2013) have found a thermal conductivity for the Earth's core that is much higher than the conventional value (Stacey & Loper, 2007), although it remains controversial (Konôpková et al., 2016; Xu et al., 2018). High conductivities make thermal convection difficult, and chemical buoyancy may provide an alternate means of driving convection in the core, depending upon its chemical composition, from early in the history of the Earth. It has been proposed that the compositional buoyancy could arise from crystallization of MgO (Badro et al., 2016; O'Rourke & Stevenson, 2016) or SiO_2 (Hirose et al., 2017) from core metal originally enriched in Si, O, and possibly Mg as a consequence of metal-silicate segregation at high pressure and temperature ($P-T$) (Badro et al., 2018; Du et al., 2017; Fischer et al., 2015; Jackson et al., 2018; Siebert et al., 2013).

The joint solubility of Si and O in liquid Fe is limited at 1 bar (O'Neill et al., 1998) (Figure 1a), which has steel-making applications. The multianvil experiments by Tsuno et al. (2013) found limited solubility also at 25 GPa. Hirose et al. (2017) extended the experiments to core pressures by demonstrating the crystallization of SiO_2 from liquid Fe-Si-O. An alternative interpretation of liquidus SiO_2 presence is liquid-liquid immiscibility in Fe-Si-O (Arveson et al., 2019), but more recent ab initio calculations found evidence of neither liquid immiscibility nor SiO_2 crystallization at ~135 GPa (Huang et al., 2019).

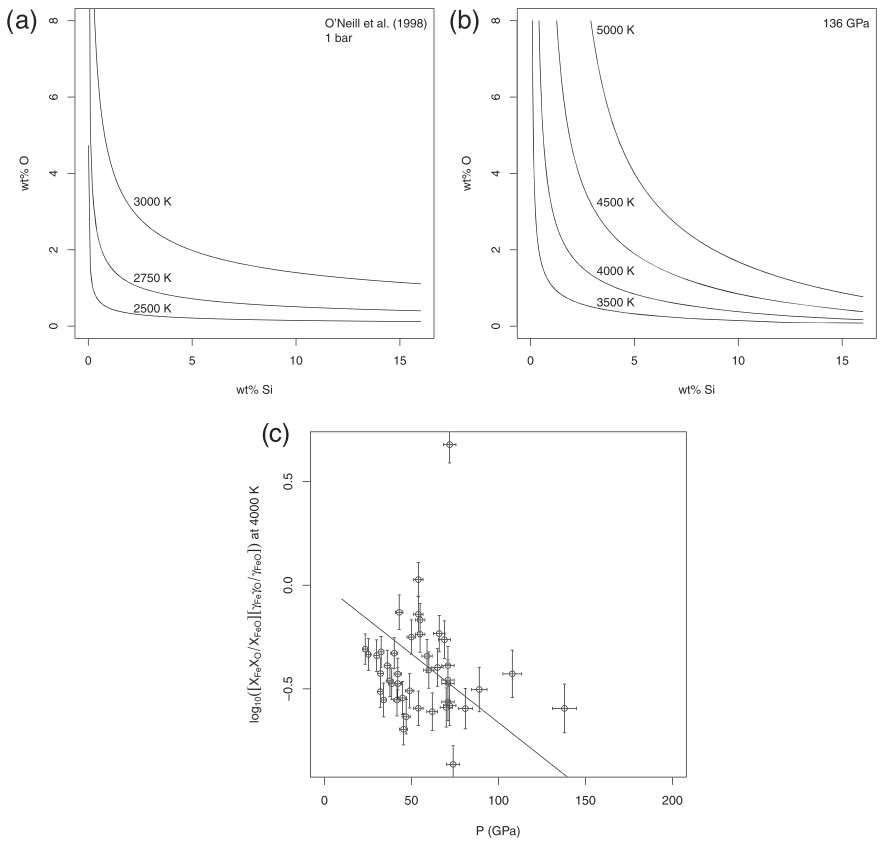

Figure 1. Si + O simultaneous solubility limits (a) at 1 bar from steel-making literature (adapted from O'Neill et al., 1998) and (b) at 136 GPa updated in this study by using recent experimental data. A negative pressure dependence of K_D^O (c) leads to decrease in the Si + O solubility with increasing P at a given T.

While the earlier thermodynamic models developed by Badro et al. (2016, 2018) explored the saturation of Mg in liquid iron, they did not consider the effect of Si and O on the uptake of Mg. In order to understand the joint SiO_2 + MgO saturation in the Earth's liquid core, we developed a thermodynamic model of joint Mg + Si + O solubility in liquid iron on the basis of all available earlier DAC experiments reported in the literature.

~~It is likely that sufficient Si and O were dissolved into the Earth's core that it may still be crystallizing SiO_2 today~~ (Hirose et al., 2017). ~~Since SiO_2 is buoyant in the deep lower mantle, a layer of SiO_2 that accumulates at the CMB is swept into the mantle, and SiO_2 expelled from the core in the early history of the Earth may now be trapped in the midlower mantle despite whole mantle flow~~ (Helffrich et al., 2018). On the other hand, a high Mg concentration in the initial core is required for MgO saturation. If it happened, possibly as a result of a high-T planetary formation event, the core might expel (Mg,Fe)-silicate melts in addition to solid SiO_2, which has geophysical and geochemical implications that we explore here.

2. Thermodynamic Model

2.1. Motivation

In order to explore the joint SiO_2 + MgO saturation in liquid Fe, we performed a preliminary melting experiment on a homogeneous Fe-Si-O-Mg sample (Fe-7.21%Si-13.84%O-1.43%Mg by weight) in a diamond-anvil cell at 25 GPa (Figure S1 in the supporting information). The sample cross section showed both quenched liquid metal and (Mg,Fe)-silicate melt at the laser-heated hot spot, coexisting with solid SiO_2. While the experiment was carried out at relatively low pressure, it shows that Fe-Si-O-Mg alloy exsolves SiO_2 crystals and (Mg,Fe)-silicate melt upon cooling, and, by extension, the core may also do so at higher pressure.

2.2. Metal-Silicate Partitioning of Mg, Si, and O

Here we thermodynamically examine the exsolution of SiO_2 and silicate melt from liquid Fe-Si-O-Mg. While we employ the previously known distribution coefficient K_D^{Si} of Si between metal and silicate (Fischer et al., 2015; Hirose et al., 2017), K_D^{Mg} of Mg is obtained from all available metal-silicate sandwiched experiments in the literature (Badro et al., 2016, 2018; Chidester et al., 2017; Du et al., 2017; Jackson et al., 2018) (see the supporting information). Due to our own experience with microprobe analyses of Mg in metal, we only use experiments whose reported Mg concentrations are ≥0.1 wt%. Self-consistent metal/silicate partitioning calculations for Mg, Si, and O in metal also require the K_D for O (Fischer et al., 2015; Hirose et al., 2017), $K_D^O = X_{Fe}^{met} X_O^{met} / X_{FeO}^{met}$, which is updated in this study by using these recent experimental data.

It is common to use exchange reactions to model metal-silicate equilibrium experiments. A generic oxidation state change reaction for dissolution of a cation M, of valence n+, in a metal (melt or solid), may be written

$$MO_{n/2} = M + \frac{n}{4} O_2.$$

Iron is the most geologically relevant metal for cation incorporation, so we can use a similar oxidation-reduction equilibrium for it, the iron (Fe)-wüstite (FeO) equilibrium,

$$2\,Fe + O_2 = 2FeO,$$

and combine equations the previous two equations to eliminate oxygen

$$MO_{n/2} + \tfrac{n}{4} \times 2Fe + \tfrac{n}{4} O_2 = M + \tfrac{n}{4} \times O_2 + \tfrac{n}{4} 2FeO$$
$$MO_{n/2} + \tfrac{n}{2} \times Fe = M + \tfrac{n}{2} FeO,$$

as, for example, did Wade and Wood (2005). The feasibility of the exchange relies on the certainty that the experimental $P-T$ can shift the iron-wüstite equilibrium sufficiently to induce detectable $MO_{n/2}$ dissociation.

In the Fe-Mg-Si-O system the incoherence of a plot of $\log(D_{Mg})$ versus $\log(f_{O_2})$ relative to the Fe-FeO buffer, which should be linear if Mg is reduced by Fe (Figure S2), shows that the oxidation state shift is difficult to achieve with the individual Mg-MgO and Si-SiO_2 equilibria and iron. This suggests that reduction of M^{n+} to M^0 by Fe is not possible in all cases due to limitations on exchange of O between the metal, silicate, and experimental environment. Hence, an alternative approach to handling the exchange reaction is required. Assuming for simplicity ideal metal and silicate mixing, we write an exchange reaction involving the Si and Mg in the metal that reads

$$\underset{\text{in metal}}{Si} + \underset{\text{in silicate}}{2MgO} = \underset{\text{in metal}}{2Mg} + \underset{\text{in silicate}}{SiO_2}$$

and which has a K_D^{ex} that reads

$$K_D^{ex} = \frac{X_{Mg}^{met^2}}{X_{Si}^{met}} \frac{X_{SiO_2}^{sil}}{X_{MgO}^{sil\ 2}}. \quad (1)$$

Using the following distribution coefficient K_D definitions for Mg and Si (which express the reactions $MgO^{sil} = Mg^{met} + O^{met}$ and $SiO_2^{sil} = Si^{met} + 2O^{met}$),

$$K_D^{Mg} = X_{Mg}^{met} X_O^{met} / X_{MgO}^{sil},\ K_D^{Si} = X_{Si}^{met} X_O^{met^2} / X_{SiO_2}^{sil}.$$

Equation 1 may be rewritten as

$$K_D^{ex} = K_D^{Mg^2} / K_D^{Si},$$

and thus (including activity coefficients)

$$K_D^{Mg^2} = K_D^{Si} \times \left[\frac{X_{Mg}^{met^2}}{X_{Si}^{met}} \frac{X_{SiO_2}^{sil}}{X_{MgO}^{sil\ 2}} \right] \left[\frac{\gamma_{Mg}^{met^2}}{\gamma_{Si}^{met}} \frac{\gamma_{SiO_2}^{sil}}{\gamma_{MgO}^{sil\ 2}} \right]$$

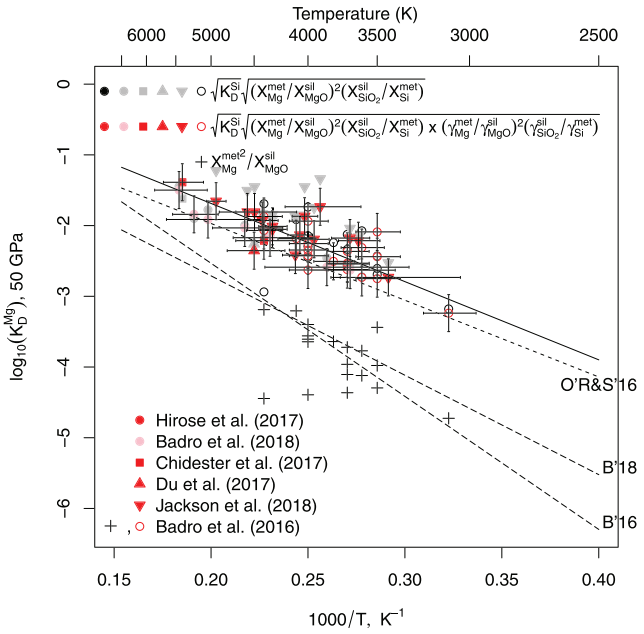

Figure 2. Metal-silicate distribution coefficient K_D for Mg. Red and black points show data without correction for metal and silicate interaction parameters (ϵ_i^j and W_{i-j}) and with correction for interaction parameters, respectively, normalized to constant $P = 50$ GPa (to remove scatter due to pressure). Full line is fit at $P = 50$ GPa; dashed lines are fits from Badro et al. (2016) and Badro et al. (2018). O'R&S is model of O'Rourke and Stevenson (2016). Crosses show Badro et al. (2016) and Badro et al. (2018) IPGP data processed with their dissolution model. Each of these data points (crosses) relocates into the point cluster when processed with our model (open circles). The present model entails higher solubility of Mg in liquid iron alloy and leads to no crystallization of MgO.

or logarithmically as

$$2\log K_D^{\mathrm{Mg}} = \log K_D^{\mathrm{Si}} + \log\left(\left[\frac{X_{\mathrm{Mg}}^{\mathrm{met}^2}}{X_{\mathrm{Si}}^{\mathrm{met}}}\frac{X_{\mathrm{SiO_2}}^{\mathrm{sil}}}{X_{\mathrm{MgO}}^{\mathrm{sil}\ 2}}\right]\left[\frac{\gamma_{\mathrm{Mg}}^{\mathrm{met}^2}}{\gamma_{\mathrm{Si}}^{\mathrm{met}}}\frac{\gamma_{\mathrm{SiO_2}}^{\mathrm{sil}}}{\gamma_{\mathrm{MgO}}^{\mathrm{sil}\ 2}}\right]\right). \quad (2)$$

This enables one to solve for K_D^{Mg} of Mg between metal and silicate with the previously known K_D^{Si} of Si in iron metal (Fischer et al., 2015; Hirose et al., 2017) (Figure 2). The K_D for Mg, Si, and O is parameterized with an expression of the form (Table S1)

$$\log_{10} K_D = a + b\frac{1}{T} + c\frac{P}{T}. \quad (3)$$

We use the ϵ model (Ma, 2001) for activity coefficients in the metal. New coefficients for Equation 3 were also determined for K_D^{O} differing from previous determinations in their use of the silicate activity coefficients estimated for fitting Equation 2.

The governing role of the internal Mg-Si exchange reaction may be seen if the experiments are plotted against f_{O_2} defined by the Si-SiO_2 buffer (Figure S3), in a manner analogous to Wade et al. (2012). The observed D_{Mg} shows the expected dependence for exchange with a 2+ cation such as Mg. What this shows is that Mg uptake by liquid iron is controlled by reduction of Mg^{2+} to Mg^0. It also shows the relative charge of the species participating in the exchange reaction through the slope of the reaction (Wade et al., 2012). The slope is consistent with a 4+ cation reducing a 2+ cation.

Badro et al. (2016, 2018) argue that Mg in silicate is dissolved as MgO in metal; indeed, data in Figure 2 show that one could draw this inference. We note, however, that oxide species in silicate melt are only thermodynamic abstractions: eutectics in, for example, the MgO-SiO_2 system do not correspond to stoichiometric proportions of the oxides. Hence, there is no reason to endow them with the physical reality implicit in a model wherein Mg is incorporated in metal as an oxide. The $\log(D_{\mathrm{Mg}})$ versus $\log(f_{O_2})$ relation supports this view (Figure S3).

Figure 2 shows a summary of the goodness of the fit to the experimental data, and a comparison to the fits of Badro et al. (2016, 2018) to a reduced data set. Our model yields significantly higher solubility of Mg in metal, essentially due to the Mg-Si interaction in the metal. Note that our model utilizes all available DAC experimental data (Badro et al., 2016, 2018; Chidester et al., 2017; Du et al., 2017; Jackson et al., 2018), which are almost the same as those used by Badro et al. (2018).

2.3. Modeling of Liquidus Phase Relations in SiO_2-MgO-FeO at the CMB

We also modeled the ternary silicate liquidus diagram by following Boukaré et al.'s (2015) model and methodology with updated values for thermochemical constants (F_0, S_0) in the liquid equations of state and solid $MgSiO_3$ constrained by newer melting experiments on the liquid endmembers, MgO, FeO, and SiO_2 (Figure S4). We use the melt activity parameterization from Boukaré et al. (2015) that recognizes the species MgO, FeO, and SiO_2 in the melt, for which a symmetric Margules mixing model is used. MgO and FeO are assumed to mix ideally in the silicate, but not MgO-SiO_2 and FeO-SiO_2, which are nonideal. Hence, the activity coefficients γ_i of the MgO, FeO, and SiO_2 melt species i are

$$\begin{aligned} RT\log\gamma_{\mathrm{MgO}} &= X_{\mathrm{SiO_2}}[(1-X_{\mathrm{MgO}})W_{\mathrm{MgO-SiO_2}} - X_{\mathrm{FeO}}W_{\mathrm{FeO-SiO_2}}], \\ RT\log\gamma_{\mathrm{FeO}} &= X_{\mathrm{SiO_2}}[-X_{\mathrm{MgO}}W_{\mathrm{MgO-SiO_2}} + (1-X_{\mathrm{FeO}})W_{\mathrm{FeO-SiO_2}}], \\ RT\log\gamma_{\mathrm{SiO_2}} &= [X_{\mathrm{MgO}}W_{\mathrm{MgO-SiO_2}} + X_{\mathrm{FeO}}W_{\mathrm{FeO-SiO_2}}](X_{\mathrm{MgO}} + X_{\mathrm{FeO}}). \end{aligned}$$

Fitting Equation 2 therefore requires the estimation of the a, b, and c parameters for K_D^{Mg}, the activity coefficients in the metal related to Mg ($\epsilon_{\mathrm{Mg}}^{\mathrm{Mg}}, \epsilon_{\mathrm{Mg}}^{\mathrm{O}}, \epsilon_{\mathrm{Mg}}^{\mathrm{Si}}$), and two interaction parameters in the liquid silicate ($W_{\mathrm{MgO-SiO_2}}$ and $W_{\mathrm{FeO-SiO_2}}$). Table S2 gives the revised thermochemical parameters.

3. Discussion

3.1. Saturation of SiO_2 in Liquid Fe

We have updated the Si + O simultaneous solubility in liquid Fe at the CMB conditions of 136 GPa (Hirose et al., 2017) by using recent experimental data (Badro et al., 2016, 2018; Chidester et al., 2017; Du et al., 2017; Jackson et al., 2018) (Figure 1b). The Si + O solubility diminishes with increasing P at a given T, which is a consequence of a negative pressure effect on K_D^{O} as demonstrated in Figure 1c.

3.2. Saturation of Mg in the Core

On the basis of K_D^{Mg} obtained above, we can calculate the concentration of Mg in metal for a variety of single stage core formation models at different pressures between 20 and 60 GPa, in equilibrium with molten silicate of bulk silicate earth composition (pyrolite or CI chondrite composition) (McDonough & Sun, 1995) (Figure S5). We use a single-stage core formation model due to its conceptual simplicity and compatibility with chemical models and constraints on core formation (Fischer et al., 2015; Siebert et al., 2013) without needing to invoke conditions in weakly constrained phenomena such as particular accretion sequences (Rubie et al., 2015). This yields robust limits on incorporation of Mg into the core that are not strongly model dependent. At any metal-silicate equilibration pressure (magma ocean depth), only 0.08–0.3 wt% Mg is dissolved in the core, and for moderate pressure (35–50 GPa), only about 0.2 wt% is.

We can also calculate the maximum concentration of MgO in the liquid core by a combination of K_D^{Mg} and K_D^{O} values (Figures S5 and 3a). The results demonstrate that at least 1.7 ± 0.5 wt% Mg is required for MgO saturation even at the present-day CMB conditions (~4,000 K). This indicates that even with the higher Mg solubility that our model entails, there is insufficient Mg to saturate it in the core (Badro et al., 2016) assuming the single-stage core formation model based on the metal-silicate partitioning of siderophile elements (Fischer et al., 2015; Siebert et al., 2013). Du et al. (2019) estimated similar amounts to ours, 1.5 wt%.

Badro et al. (2016) invoked addition of Mg through the high temperatures generated in a giant impact, using a different Mg dissolution model in liquid Fe than ours (Figure 2). With our revised K_D expression, for Mg to be crystallizing from the core requires a minimum C_{Mg} of 1.7 ± 0.5 wt% Mg in the core at end-accretion, postimpact time. Taking the high Mg content estimate from the single stage formation model as the preimpact core Mg concentration C^0_{Mg}, we ask how much additional Mg must be added by the impactor to the core. The most effective way is for the impactor's total metal content to be reequilibrated with silicate in the target's magma ocean. If $D_{\mathrm{Mg}} = C_{\mathrm{Mg}}/C_{\mathrm{MgO}}$ is the metal-silicate distribution coefficient for Mg, an Mg mass balance is thus

$$\underbrace{C_{\mathrm{Mg}} f_c M_\oplus}_{\text{Mg mass in present core}} = \underbrace{C^0_{\mathrm{Mg}} f_c (M_\oplus - M_i)}_{\text{Mg mass in pre-impact core}} + \underbrace{D_{\mathrm{Mg}} C^i_{\mathrm{MgO}} M_\oplus (1 - f_c) f_{mo}}_{\text{Mg mass in magma ocean}\rightarrow\text{core}},$$

where f_c is the fraction of Earth mass $M_\oplus$ that is the core (0.32), M_i is the impactor mass, and f_{mo} is the mass fraction of silicate that makes up the magma ocean, a number between 0.6 and 0.75 for depths corresponding to 35–50 GPa (Siebert et al., 2013); we also assume the same fraction of metal in the Earth and impactor. The impact must supply this by extracting Mg from the combined silicate of the impactor and target. C_{MgO} is the mantle's MgO mass concentration, or ~38 wt% (McDonough & Sun, 1995). Hence, $D_{\mathrm{Mg}} \approx C^i_{\mathrm{Mg}}/38$. We use the expression for D to K_D conversion in peridotite and then the K_D^{Mg} coefficients from Table S1 to solve for the range of T values that will yield sufficient Mg incorporation into the core and find that temperatures of 5,200–5,600 K (5,323 K mean) are required, which are 1,000–2,000 K above the liquidus temperature at the base of the magma ocean (Fiquet et al., 2010) (Figure S5, top). The conditions are not as extreme as those required in a giant impact scenario but require late addition of a single batch of metal equilibrated with the silicate in a super-liquidus magma ocean. Because the dilution factor is close to 1 for lithophile D values (Deguen et al., 2014), the consideration of partial equilibration with metal does not materially affect these conclusions.

Another way to have >1.7 wt% Mg in the core could be the assimilation of silicate into the liquid core as a result of turbulent mixing at the time of a giant impact. The fluid mixing experiments by Landeau et al. (2016) demonstrated a possibility that a molten impactor core entrained a certain amount of silicate (mostly melt) before penetrating into the proto-core of the Earth. If this is the case, silicate was intermingled with liquid metal at small scales, and Si, O, and Mg in the silicate dissolved into the core, depending on temperature;

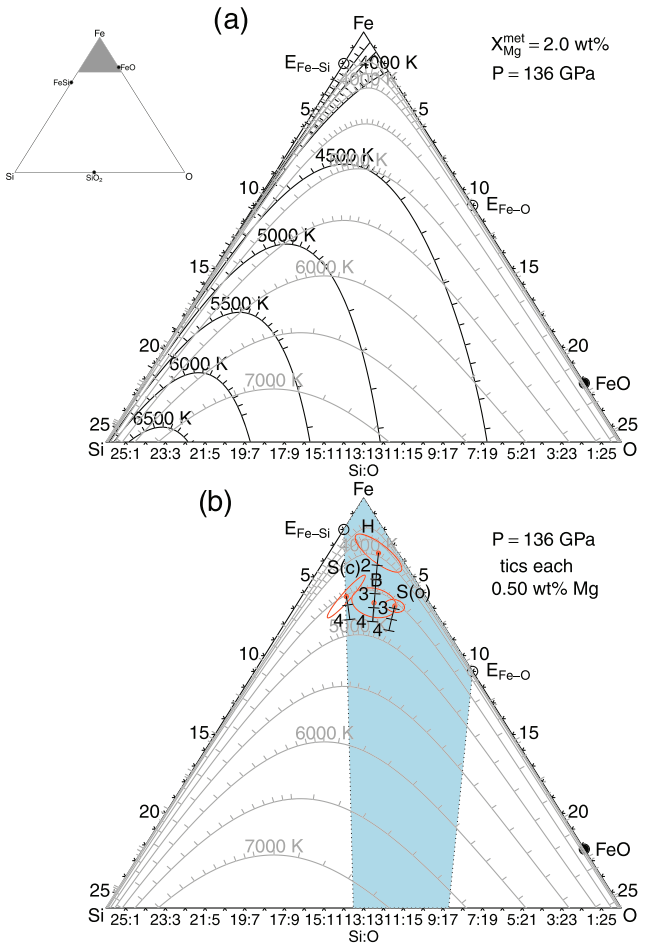

Figure 3. Joint MgO and SiO_2 solubility in liquid iron at the CMB and core crystallization paths. (a) Dark lines show limits of MgO solubility at different temperatures for core metal containing 2 wt% Mg; gray lines show limits of SiO_2 solubility. (b) Evolution paths of core composition by joint exsolution of (Mg,Fe)O and SiO_2 components (silicate melt + solid SiO_2), calculated from various present-day core composition estimates; S(c), S(o), Siebert et al. (2013) constant and oxidized compositions; B, Badro et al. (2015); H, Hirose et al. (2017). Numbers indicate X_{Mg}^{met} and T, and tics mark loss each 0.5 wt%. Pale blue region shows compositional limits given by the present Earth core structure due to inner core crystallization of Fe rather than FeSi (Ozawa et al., 2016) or FeO (Morard et al., 2017); $E_{Fe\text{-}Si}$ and $E_{Fe\text{-}O}$ are positions of Fe-Si and Fe-O eutectics at CMB conditions that limit the inner core to crystallizing an iron-rich alloy.

indeed, 3,500 K at the CMB is high enough to dissolve 2 wt% Mg (Figure 3a). In order to add >1.5 wt% Mg to the core by this mechanism, it is necessary for the impactor core to entrain pyrolitic molten silicate whose mass corresponds to >6% of the entire core (pyrolite contains 23 wt% Mg) (McDonough & Sun, 1995). Assuming a Mars-sized impactor with 10% of Earth mass and 1/2-1/3 metal volume, the approximation from Landeau et al.'s (2016) turbulent mixing experiments that the volume of silicate melt entrained with metal is roughly equal to the metal volume leads to the assimilation of silicate with 8–14% (more than 6%) of core mass. Note that the assimilation of 6 wt% pyrolitic material into the core does not change the chemical composition of the silicate mantle and thus does not affect estimates of the conditions for core formation (Fischer et al., 2015; Siebert et al., 2013). It is also noted that it increases Si and O concentrations in the core only by 1.3 and 2.6 wt%, respectively (pyrolite contains 21 wt% Si and 44 wt% O) (McDonough & Sun, 1995).

3.3. Joint Saturation of MgO + SiO_2 and the Exsolution of Silicate Melt

Our model defines the solubility limits of MgO and SiO_2 in core metal at present-day CMB conditions of 136 GPa (Figure 3, blue shaded area). Only with $X_{Mg}^{met} > 1.7 \pm 0.5$ wt% will MgO and SiO_2 jointly precipitate from the core at temperatures in the expected contemporary range for the CMB (3,500 K $\leq T_{CMB} \leq$ 4,200 K) (Boukaré et al., 2015; Nomura et al., 2014). This is feasible given the core formation scenario provided there is late addition of Mg (Figure S5). Reverse crystallization paths calculated from a variety of feasible present-day core compositions (Badro et al., 2015; Hirose et al., 2017; Siebert et al., 2013) lead to end-accretion core compositions limited by an initial Mg content of < 4 wt% (Figure 3b). This suggests a low-Si (<5 wt%), high-O (~6 wt%) core that expelled 1–2.5 wt% Mg and Si + O as SiO_2 evolved to its present Mg content of 1.5–3.3 wt% Mg.

SiO_2 always saturates before MgO in the composition range explored (Figure 3a). Loss of Si + O as liquid or solid SiO_2 as the core cools eventually leads to an (Mg,Fe)-silicate (SiO_2 + MgO + FeO) being expelled. This occurs when the MgO saturation curve is reached. As the core cools, the isopleths of MgO and SiO_2 saturation move along the trajectories shown in Figure 3b, and the rates of MgO and SiO_2 loss with the change in temperature give the composition of the silicate expelled from the metal. It includes some FeO, and the compositions are shown as the pink region in the SiO_2-MgO-FeO ternary diagram in Figure 4.

The state of the silicates expelled from the core depends on temperature and the ternary liquidus phase relations in SiO_2-MgO-FeO (Figure 4). The SiO_2-MgO-FeO ternary liquidus phase relations show that the (Mg, Fe)-silicate exsolved from the core is composed of melt ± solid SiO_2 when the core saturates with MgO at temperatures ~4,450 ± 225 K. Note that eutectic melting temperature in the $SiO_2 - MgSiO_3$ binary is much lower than the melting point of SiO_2 (Baron et al., 2017), leading to the formation of melt once SiO_2 and MgO are jointly expelled.

3.4. Evolution of Silicate Melts and the Formation of ULVZs

The silicate melt crystallizes SiO_2 as it cools down to 4,275 ± 225 K, and then (Mg,Fe)SiO_3 bridgmanite will also cocrystallize (Figure 4). If the solid and liquid separate, the liquid composition will evolve along the cotectic leading to a ternary liquid minimum of 3,848 ± 170 K. If the present-day CMB temperature is higher, liquid silicate will be present there. Some useful estimates of the amount of solid formed from silicate expelled from the core may be derived from the liquid composition at the ternary minimum and the liquid composition expelled from the core. If the core exsolves between 1 and 2.5 wt% Mg of composition

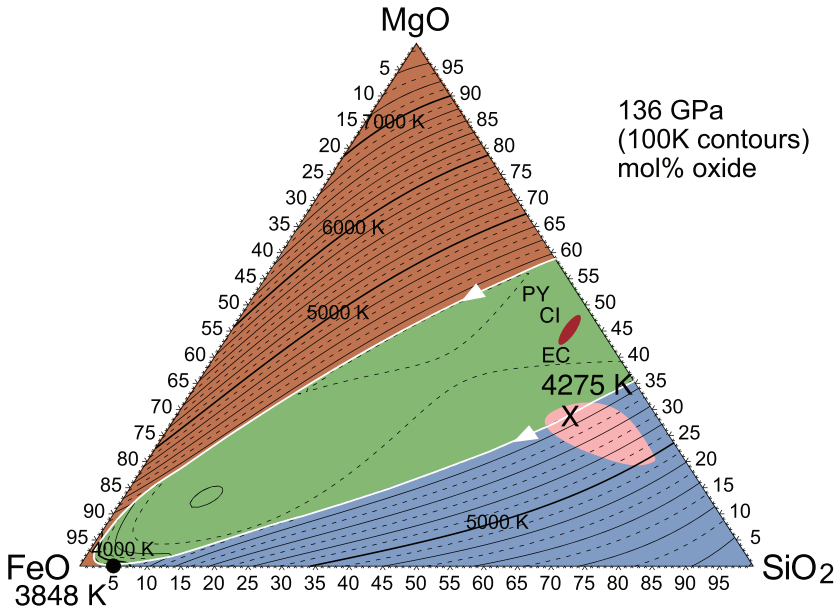

Figure 4. Ternary liquidus field relations in the SiO_2-MgO-FeO system at the CMB. Pink region outlines the composition of (Mg,Fe)-silicate exsolved by the cooling core. $MgSiO_3 - SiO_2$ eutectic is 4,300 ± 225 K. The liquid silicate will crystallize SiO_2 (reaching X) and then bridgmanite + SiO_2 (descending to the ternary minimum along the white line). Red lozenge shows compositional Mg/(Mg + Fe) ratio of bridgmanite crystallized. If the silicate crystallizes as a batch, the result will be a solid consisting of SiO_2 ± bridgmanite at ~4,275 ± 225 K (X). If the silicate undergoes fractional crystallization as it cools on release from the core and ascent to the CMB, the liquid will evolve to the ternary minimum at 3,848 ± 170 K (labeled point). This would give rise to molten silicate at the CMB if it is at higher *T*. PY, CI, and EC show compositions of mantle silicate (pyrolite, CI, and enstatite chondrites) for comparison (Javoy et al., 2010; McDonough & Sun, 1995).

68 mol% $(Mg_{0.9}Fe_{0.1})SiO_3$ and 32 mol% SiO_2 (Figure 4, "X"), between 98 and 99 wt% must be lost to the mantle as solids. The residual liquid volume corresponds to a global layer thickness between 1 and 3 km at the CMB (using the density of metal at the CMB and silicate at the base of the mantle as bounds on the silicate liquid density; a more detailed comparison is not possible due to the EOS used in the thermodynamic model). If concentrated by lateral flow of the lowermost mantle above the CMB, it could locally form thicker, seismically visible melt regions; ~5 km is thought to be the detection limit for ultralow-velocity zone (ULVZ) thickness (Yu & Garnero, 2018). Irrespective of melt presence, the solids would be bridgmanite (or hiroseite; FeO-rich $(Mg,Fe)SiO_3$ perovskite) + SiO_2. Volumetrically, solids crystallized from the core by loss of 1–2.5 wt% Mg would form a volume of 2.9–7.2% of the mantle. It is also possible that eventual crystallization of FeO-rich melt produces ferropericlase-rich regions with ULVZ properties (Wicks et al., 2010).

Direct transfer of silicate material from the core to the mantle would also leave the mantle with the siderophile trace elements such as Mo, W, and Pt carried by the silicate. Rizo et al. (2019) show evidence for this in Archean and modern lavas. In the case of Mo, the combination of its increasing lithophile tendency with pressure (Cottrell et al., 2009; Wade et al., 2012) and its concentrations in the core and mantle (Willbold & Elliott, 2017) indicate that mantle $\delta^{98/95}$Mn would be changed by a factor of ~3 times more than analytical precision, a not insignificant isotopic model detail. For W the implications are not as clear, but the pressure effect on the W-WO_2 buffer (Shofner et al., 2016) also suggests a waning of siderophile tendency for W at core conditions, potentially complicating inferences of core formation from the W-Hf system (Nimmo & Kleine, 2015). Transfer of radiogenic Pt from the core, affecting Os isotope systematics (Humayun, 2011), might arise if silicate from the core retains more Pt than under magma ocean conditions.

ULVZs at the CMB are commonly attributed to partially molten material (Williams & Garnero, 1996), but their proximity to large low shear-velocity provinces (LLSVPs) that extend upward into the mantle (Garnero & McNamara, 2008) led to the inference that the melting was due to either excessively hot or compositionally fertile material on the mantle side of the CMB. If the core is saturated in Mg, however, our models rather imply that ULVZs are a byproduct of the core's evolution and that their positions, occasionally unconnected

to LLSVPs (Yu & Garnero, 2018), might be controlled by convective incorporation of the residual solids and liquid into the mantle.

4. Conclusions

We developed a thermodynamic model describing the SiO_2 and MgO saturation in molten Fe under Earth's core conditions on the basis of all available earlier DAC metal-silicate partitioning experiments in the literature. The results show that the effects of Si and O in liquid iron enhances the retention of Mg in the metal.

Our model indicates that SiO_2 always saturates in the core before MgO, in the plausible core compositional range explored. With $<1.7 \pm 0.5$ wt% Mg, MgO saturation does not occur even with core cooling to ~4,000 K at CMB. With higher amounts of Mg in the initial core, which could have happened as a result of the addition of an impactor core that equilibrated with silicate at $5{,}323^{+300}_{-100}$ K or the assimilation of silicate into the liquid core at the time of a giant impact, joint SiO_2 + MgO saturation takes place, leading to the exsolution of solid SiO_2 + Mg-silicate melts from the core. Note that the eutectic temperature in the $MgSiO_3 - SiO_2$ system is $4{,}300 \pm 225$ K at the CMB, an upper bound for melts to exist because other mantle components will lower it.

The exsolution of solid SiO_2 + silicate melts may be a main material transport from the core into the mantle, which has been inferred from geochemistry. Our revised liquidus phase relations in SiO_2-MgO-FeO ternary system at 136 GPa indicate that the core-derived silicate melts undergo fractional crystallization and evolve toward the ternary minimum close to FeO. Such evolved melts are dense and possibly form the ULVZ currently observed above the CMB.

Data Availability Statement

Data for Figure 2 are reported in Hirose et al. (2017), Badro et al. (2018), Chidester et al. (2017), Du et al. (2017), and Badro et al. (2016). Full analyses in Table S3 available online (from https://doi.org/10.5281/zenodo.3893072).

Acknowledgments
This work was supported by the JSPS Grant 16H06285 to K. H. We thank the reviewers for improving the manuscript.

References

Arveson, S. M., Deng, J., Karki, B. B., & Lee, K. K. M. (2019). Evidence for Fe-Si-O liquid immiscibility at deep Earth pressures. *Proceedings of the National Academy of Sciences*, *116*, 10,238–10,243.

Badro, J., Aubert, J., Hirose, K., Nomura, R., Blanchard, I., Borensztajn, S., & Siebert, J. (2018). Magnesium partitioning between Earth's mantle and core and its potential to drive an early exsolution geodynamo. *Geophysical Research Letters*, *45*, 13,240–13,248. https://doi.org/10.1029/2018GL080405

Badro, J., Brodholt, J. P., Piet, H., Siebert, J., & Ryerson, F. J. (2015). Core formation and core composition from coupled geochemical and geophysical constraints. *Proceedings of the National Academy of Sciences*, *112*, 12,310–12,314.

Badro, J., Siebert, J., & Nimmo, F. (2016). An early geodynamo driven by exsolution of mantle components from Earth's core. *Nature*, *536*, 326–328.

Baron, M. A., Lord, O. T., Myhill, R., Thomson, A. R., Wang, W., Trønnes, R., & Walter, M. J. (2017). Experimental constraints on melting temperatures in the MgO-SiO_2 system at lower mantle pressures. *Earth and Planetary Science Letters*, *472*, 186–196.

Boukaré, C.-E., Ricard, Y., & Fiquet, G. (2015). Thermodynamics of the MgO-FeO-SiO_2 system up to 140 GPa: Application to the crystallization of Earth's magma ocean. *Journal of Geophysical Research: Solid Earth*, *120*, 6085–6101. https://doi.org/10.1002/2015JB011929

Chidester, B. A., Rahman, Z., Righter, K., & Campbell, A. J. (2017). Metal-silicate partitioning of U: Implications for the heat budget of the core and evidence for reduced U in the mantle. *Geochimica et Cosmochimica Acta*, *199*, 1–12.

Cottrell, E., Walter, M. J., & Walker, D. (2009). Metal-silicate partitioning of tungsten at high pressure and temperature: Implications for equilibrium core formation. *Earth and Planetary Science Letters*, *281*, 275–287.

de Koker, N., Steinle-Neumann, G., & Vlček, V. (2012). Electrical resistivity and thermal conductivity of liquid Fe alloys at high P and T, and heat flux in Earth's core. *Proceedings of the National Academy of Sciences*, *109*, 4070–4073.

Deguen, R., Landeau, M., & Olson, P. (2014). Turbulent metal-silicae mixing, fragmentation, and equilibratin in magma oceans. *Earth and Planetary Science Letters*, *191*, 274–287.

Du, Z., Boujibar, A., Driscoll, P., & Fei, Y. (2019). Experimental constraints on an MgO exsolution-driven dynamo. *Geophysical Research Letters*, *44*, 7379–7385. https://doi.org/10.1029/2019GL083017

Du, Z., Jackson, C., Bennett, N., Driscoll, P., Deng, J., Lee, K. M., et al. (2017). Insufficient energy from MgO exsolution to power early geodynamo. *Geophysical Research Letters*, *44*, 11,376–11,381. https://doi.org/10.1002/2017GL075283

Fiquet, G., Auzende, A. L., Siebert, J., Corgne, A., Bureau, H., Ozawa, H., & Garbarino, G. (2010). Melting of peridotite to 140 Gigapascals. *Science*, *329*, 1516–1518.

Fischer, R. A., Nakajima, Y., Campbell, A. J., Frost, D. J., Harries, D., Langenhorst, F., et al. (2015). High pressure metal-silicate partitioning of Ni, Co, V, Cr, Si, and O. *Geochimica et Cosmochimica Acta*, *167*, 177–194.

Garnero, E. J., & McNamara, A. K. (2008). Structure and dynamics of Earth's lower mantle. *Science*, *320*, 626–628.

Gomi, H., Ohta, K., Hirose, K., Labrosse, S., Caracas, R., Verstraete, M. J., & Hernlund, J. W. (2013). The high conductivity of iron and thermal evolution of the Earth's core. *Physics of the Earth and Planetary Interiors*, *224*, 88–103.

Helffrich, G., Ballmer, M., & Hirose, K. (2018). Core-exsolved SiO_2 dispersal in the Earth's mantle. *Journal of Geophysical Research: Solid Earth*, *123*, 176–188. https://doi.org/10.1002/2017JB014865

Hirose, K., Morard, G., Sinmyo, R., Umemoto, K., Hernlund, J., Helffrich, G., & Labrosse, S. (2017). Crystallization of silicon dioxide and compositional evolution of the Earth's core. *Nature*, *543*, 99–102.

Huang, D., Badro, J., Brodholt, J., & Li, Y. (2019). Ab initio molecular dynamics investigation of molten Fe-Si-O in Earth's core. *Geophysical Research Letters*, *46*, 6397–6405. https://doi.org/10.1029/2019GL082722

Humayun, M. (2011). A model for osmium isotopic evolution of metallic solids at the core-mantle boundary. *Geochemistry, Geophysics, Geosystems*, *12*, Q03007. https://doi.org/10.1029/2010GC003281

Jackson, C. R. M., Bennett, N. R., Du, Z., Cottrell, E., & Fei, Y. (2018). Early episodes of high-pressure core formation preserved in plume mantle. *Nature*, *553*, 491–495.

Javoy, M., Kaminski, E., Guyot, F., Andrault, D., Sanloup, C., Moreira, M., et al. (2010). The chemical composition of the Earth: Enstatite chondrite models. *Earth and Planetary Science Letters*, *293*, 259–268.

Konôpková, Z., McWilliams, R. S., Gómez-Pérez, N., & Goncharov, A. F. (2016). Direct measurement of thermal conductivity in solid iron at planetary core conditions. *Nature*, *534*, 99–101.

Landeau, M., Olson, P., Deguen, R., & Hirsh, B. H. (2016). Core merging and stratification following giant impact. *Nature Geoscience*, *9*, 786–789.

Ma, Z. (2001). Thermodynamic description for concentrated metallic solutions using interaction parameters. *Metallurgical and Materials Transactions B*, *32*, 87–103.

McDonough, W. F., & Sun, S.-s. (1995). The composition of the Earth. *Chemical Geology*, *120*, 223–253.

Morard, G., Andrault, G., Antonangeli, D., Nakajima, Y., Auzende, A. L., Boulard, E., et al. (2017). Fe-FeO and Fe-Fe_3C melting relations at Earth's core-mantle boundary conditions: Implications for a volatile-rich or oxygen-rich core. *Earth and Planetary Science Letters*, *473*, 94–103.

Nimmo, F., & Kleine, T. (2015). Early differentiation and core formation: Processes and timescales. In J. Badro & M. J. Walter (Eds.), *The Early Earth: Accretion and Differentiation* (pp. 83–102). Washington DC: American Geophysical Union.

Nomura, R., Hirose, K., Uesugi, K., Ohishi, Y., Tsuchiyama, A., Miyake, A., & Ueno, Y. (2014). Low core-mantle boundary temperature inferred from the solidus of pyrolite. *Science*, *343*, 522–525.

O'Neill, H. St. C., Canil, D., & Rubie, D. C. (1998). Oxide-metal equilibria to 2500° C and 25 GPa: Implications for core formation and the light component in the Earth's core. *Journal of Geophysical Research*, *103*, 12,239–12,260.

O'Rourke, J. G., & Stevenson, D. J. (2016). Powering Earth's dynamo with magnesium precipitation from the core. *Nature*, *529*, 387–389.

Ohta, K., Kuwayama, Y., Hirose, K., Shimizu, K., & Ohishi, Y. (2016). Experimental determination of the electrical resistivity of iron at Earth's core conditions. *Nature*, *534*, 95–98.

Ozawa, H., Hirose, K., Yonemitsu, K., & Ohishi, Y. (2016). High-pressure melting experiments on Fe-Si alloys and implications for silicon as a light element in the core. *Earth and Planetary Science Letters*, *456*, 47–54.

Pozzo, M., Davies, C., Gubbins, D., & Alfè, D. (2013). Transport properties for liquid silicon-oxygen-iron mixtures at Earth's core conditions. *Physical Review B*, *87*, 14110. https://doi.org/10.1103/PhysRevB.87.014110

Rizo, H., Andrault, D., Bennett, N. R., Humayun, M., Brandon, A., Vlastelic, I., et al. (2019). ^{1}82W evidence for core-mantle interaction in the source of mantle plumes. *Geochemical Perspectives Letters*, *11*, 6–11.

Rubie, D. C., Jacobson, S. A., Morbidelli, A., O'Brien, D. P., Young, E. D., de Vries, J., et al. (2015). Accretion and differentiation of the terrestrial planets with implications for the compositions of early-formed Solar System bodies and accretion of water. *Icarus*, *248*, 89–108.

Seagle, C., Cottrell, E., Fei, Y.-W., Hummer, R., & Prakapenka, V. B. (2013). Electrical and thermal transport properties of iron and iron-silicon alloy at high pressure. *Geophysical Research Letters*, *40*, 5377–5381. https://doi.org/10.1002/2013GL057930

Shofner, G. A., Campbell, A. J., Danielson, L. R., Righter, K., Fischer, R. A., Wang, Y., & Prakapenka, V. (2016). The W-WO2 oxygen fugacity buffer (WWO) at high pressure and temperature: Implications for f O_2 buffering and metal-silicate partitioning. *American Mineralogist*, *101*, 211–221.

Siebert, J., Badro, J., Antonangeli, D., & Ryerson, F. J. (2013). Terrestrial accretion under oxidizing conditions. *Science*, *339*, 1194–1197.

Stacey, F. D., & Loper, D. E. (2007). A revised estimate of the conductivity of iron alloy at high pressure and implications for the core energy balance. *Physics of the Earth and Planetary Interiors*, *161*(1–2), 13–18. https://doi.org/10.1016/j.pepi.2006.12.001

Tsuno, K., Frost, D. J., & Rubie, D. C. (2013). Simultaneous partitioning of silicon and oxygen into the Earth's core during early Earth differentiation. *Geophysical Research Letters*, *40*, 66–71. https://doi.org/10.1029/2012GL054116

Wade, J., & Wood, B. J. (2005). Core formation and the oxidation state of the Earth. *Earth and Planetary Science Letters*, *236*, 78–95.

Wade, J., Wood, B., & Tuff, J. (2012). Metal-silicate partitioning of Mo and W at high pressures and temperatures: Evidence for late accretion of sulphur to the Earth. *Geochimica et Cosmochimica Acta*, *85*, 58–74.

Wicks, J. K., Jackson, J. M., & Sturhahn, W. (2010). Very low sound velocities in iron-rich (Mg,Fe)O: Implications for the core-mantle boundary region. *Geophysical Research Letters*, *37*, L15304. https://doi.org/10.1029/2010GL043689

Willbold, M., & Elliott, T. (2017). Molybdenum isotope variations in magmatic rocks. *Chemical Geology*, *449*, 253–268.

Williams, Q., & Garnero, E. (1996). Seismic Evidence for Partial Melt at the Base of Earth's Mantle. *Science*, *273*, 1528–1530.

Xu, J., Zhang, P., Haule, K., Minar, J., Wimmer, S., Ebert, H., & Cohen, R. E. (2018). Thermal conductivity and electrical resistivity of solid iron at Earth's core conditions from first principles. *Physical Review Letters*, *121*, 96601.

Yu, S., & Garnero, E. (2018). Ultralow Velocity Zone Locations: A Global Assessment. *Geochemistry, Geophysics, Geosystems*, *19*, 396–414. https://doi.org/10.1002/2017GC007281

Supporting Information for "Thermodynamical Modeling of Liquid Fe-Si-Mg-O: Molten Magnesium Silicate Release from the Core"

George Helffrich[1], Kei Hirose[1,2], Ryuichi Nomura[1]*

[1]Earth-Life Science Institute, Tokyo Institute of Technology, 2-12-1 Ookayama I7E-312, Meguro-ku, Tokyo 152-8550, Japan

[2]Department of Earth and Planetary Science, The University of Tokyo, Bunkyo-ku, Tokyo 113-0033, Japan

Contents of this file

Additional methodological information

The thermodynamic model developed in this study employed previous DAC experimental data in the literature. They include seven metal-silicate sandwiched experiments (runs #002–43R, #001–43, #003–41, #005–43, #003–42, #007–47, and #006–43) reported in Badro et al. (2018). Since their metal and silicate compositions were not fully given, here we provide EPMA analyses (Table S3).

The silicate melts formed in these experiments included relatively high concentrations of K_2O, but it is actually a minor silicate melt component on a molar basis due to K_2O's high molecular weight. The effect of K_2O on the metal-silicate partitioning of Si may be estimated through the change in nbo/t of silicate melt (Ricolleau et al., 2011). For example, the presence of 9.4 wt% K_2O in run #002–43R is equivalent to temperature increase in $\sim$100 K. Ricolleau and others did not find the effect of nbo/t on the partitioning of O. The Mg partitioning in these experiments is consistent with other data obtained with K-free silicates (Figure S3), suggesting that the effect of K_2O is minimal.

We also tried to determine the carbon content in quenched molten alloy heated to 5230 K at 138 GPa (run #007–47). FE-EPMA analysis using the LDE2 analyzer crystal and Fe_3C as a standard showed 2200$\pm$3000 ppm C in quenched liquid metal, considering that the abundance at unheated metal part as a background level. Such concentration is much smaller than up to $\sim$10 wt% C in metal in previous studies that examined the effect of carbon on metal-silicate partitioning of siderophile elements (Wade & Wood, 2005; Mann et al., 2009).

The recent experiments by Arveson, Deng, Karki, and Lee (2019) reported liquid-liquid immiscibility in Fe-Si-O. The starting material used by Arveson and others was an oxygen-free Fe-Si alloy instead of Fe-Si-O; the source of oxygen was uncontrolled, but could be H_2O that is easily adsorbed on the KBr pressure medium or introduced during cryogenic loading of Ar. If this is the case, hydrogen should have been incorporated into liquid Fe alloys and might have caused liquid immiscibility. While Arveson et al. (2019) also reported ab initio calculations that support liquid-liquid immiscibility, more recent ones by Huang, Badro, Brodholt, and Li (2019) did not obtain any indications of liquid immiscibility nor SiO_2 crystallization from liquid Fe-Si-O at $\sim$135 GPa. It is possible that the number of atoms was not enough and simulation time was too short for the SiO_2 crystallization (Sun et al., 2018) in both of the theoretical calculations. Since limited Si+O joint solubility in liquid Fe and the SiO_2 crystallization from liquid Fe-Si-O have been well established at 1 bar in steel making literature (Figure 1a), one possible way to validate these or any other computationally-based SiO_2 crystallization scenarios would be to reproduce the well-known 1-bar behavior. We would welcome evidence from computational crystallization studies that they can reproduce known Fe liquid metallurgical phenomena.

Additional fitting information

We incorporate reported temperature uncertainties in the fitting process, but due to the various practices of individual experimental groups to estimate the pressure in DAC experiments, we use a nominal uncertainty of 5%. For a variety of reasons, compositional uncertainties are assumed to be 3%. They are not always reported (e.g. when studies give normalized mole fractions), they are not rigorously quantifiable due to corrections for carbon presence in the runs and run product analyses (see above), and when elements other than Fe, Mg, Si and O are normalized out of the reported analyses, it becomes difficult to formally propagate analytical uncertainties to the renormalized values.

In order to avoid introducing additional, poorly-constrained parameters into the estimation procedure, we re-normalize the analyses to molar proportions of Fe, Si, Mg and O before fitting; this omits the following other elements:

Jackson, Bennett, Du, Cottrell, and Fei (2018): Al, Ca, K, S, I, Re;

Du et al. (2017): Al, Ca, S, C, Re;

Badro et al. (2018) ELSI experiments: Al, Ca, K, Na, S;

Badro et al. (2018) IPGP experiments: Al, S, C;

Badro, Siebert, and Nimmo (2016): Al, Ca;

Chidester, Rahman, Righter, and Campbell (2017): Al, Ca, S, U, Th;

Hirose et al. (2017): none.

We justify this based on their being high molecular weight substances (I, Ca, K, Re, U, Th) which contribute low mole fractions to the starting materials (see previous section) or being elements with negligible partitioning into metal (Al, Ca, K, Na). The main impact of these simplifications is on the uncertainty in the metal composition, which the 3% adequately captures for fitting purposes. Post-hoc justification of the procedure may be seen in Figure 2, which shows that experiments with no elements other than Fe, Mg, Si and O may be modeled as well as those with minor other species in metal and silicate.

We adopt the same standard state for alloying elements used by Badro et al. (2018): the element infinitely diluted in liquid iron. As those authors explained, the *a* term in equation (3) accounts for the small shift in standard state from the pure element.

The thermodynamic properties of silicate melt play roles in both the saturation model in the metal (equation (2)) and the calculation of the liquidus relations (Figure 4). These properties should, in principle, be the same, so we attempted to find mixing parameters that fit the experimental metal-silicate partitioning data and experimental determinations of the melting silicate relations in MgO-FeO-SiO_2 (Boukaré et al., 2015; Baron et al., 2017). Unfortunately,

*Now at Hakubi Center/Graduate School of Human and Environmental Studies, Kyoto University, Sakyo-ku, Kyoto 606-8501, Japan

0094-8276/20/$5.00

using W_{i-j} estimates from the metal-silicate partitioning experiments yields inconsistent melting relations in the silicate system. Also, fitting the metal-silicate partitioning experiments using the W_{i-j}s found by Boukaré et al. (2015) significantly worsens the fit compared to that shown in Figure 2. We attribute this to the highly simplified pressure parameterization in the K_D expression (equation 3). The uncertainties for $W_{MgO-SiO_2}$ and $W_{FeO-SiO_2}$, ε^{Mg}_{Mg} and ε^{O}_{Mg} are quite large, so their values are taken to be zero on account of their being unconstrained by the data (Table S1).

Uncertainty estimation

Thermodynamic datasets are designed to reproduce a set of well-calibrated experimental phase equilibria in an internally consistent way. Consequently, uncertainties in individual parameters are highly correlated with other parameters in the dataset and may not be selectively varied. Moreover, there are systematic error sources in the dataset that arise from the choice of equilibria to fit, and the parameterization of functions used to express free energy, heat capacity, the pressure dependence of volume, etc. On this latter point, we note that Boukaré et al. (2015) chose to use the Murnaghan equation as the pressure equation of state, which is known to be unreliable at CMB pressures (Poirier, 2000). Our own model extends that of Boukaré et al. (2015), which compelled us to also use it. This prevents us from comparing calculated densities and seismic wavespeeds to geophysical models like PREM, though those values are delivered by the model.

Consequently, we estimated uncertainties in our modeling results by varying particular inputs to it. In particular, we estimated the uncertainty in the solubility of Mg in liquid iron alloy by a probabilistic selection of 500 points within the error ellipses of the estimated core compositions shown in Fig. 3 and derived the uncertainty from the standard deviation of the sample set.

We estimated uncertainties in the key eutectic temperatures in the ternary silicate melting model by varying the relevant melting curves within their reported experimental uncertainties at near-CMB conditions. $FeO-SiO_2$ is fairly well constrained by experiments (to $\sim \pm$ 180 K), but $MgO-SiO_2$ is not. We estimate an upper bound of 5500 K for $MgSiO_3$ melting (Di Paola & Brodholt, 2016). We then vary silicate $W_{MgO-SiO_2}$ and $W_{FeO-SiO_2}$ to align the thermodynamic data with the apropriate melting condition, and then re-calculate the eutectic temperatures. This leads to uncertainties of $\pm$ 225 K in $MgSiO_3-SiO_2$ and $\pm$ 170 K for $FeO-SiO_2$.

Additional references cited

Arveson, S. M., Deng, J., Karki, B. B., & Lee, K. K. M. (2019). Evidence for Fe-Si-O liquid immiscibility at deep Earth pressures. *Proc. Nat. Acad. of Sci.*, *116*, 10238-10243.

Badro, J., Aubert, J., Hirose, K., Nomura, R., Blanchard, I., Borensztajn, S., & Siebert, J. (2018). Magnesium partitioning between Earth's mantle and core and its potential to drive an early exsolution geodynamo. *Geophys. Res. Lett.*, *45*. doi: https://doi.org/10.1029/2018GL080405

Badro, J., Siebert, J., & Nimmo, F. (2016). An early geodynamo driven by exsolution of mantle components from Earth's core. *Nature*, *536*, 326-328.

Baron, M. A., Lord, O. T., Myhill, R., Thomson, A. R., Wang, W., Trønnes, R., & Walter, M. J. (2017). Experimental constraints on melting temperatures in the $MgOSiO_2$ system at lower mantle pressures. *Earth Planet. Sci. Lett.*, *472*, 186-196.

Boukaré, C.-E., Ricard, Y., & Fiquet, G. (2015). Thermodynamics of the MgO-FeO-SiO_2 system up to 140 GPa: Application to the crystallization of Earth's magma ocean. *J. Geophys. Res.*, *120*, 6085-6101.

Chidester, B. A., Rahman, Z., Righter, K., & Campbell, A. J. (2017). Metal-silicate partitioning of U: Implications for the heat budget of the core and evidence for reduced U in the mantle. *Geochim. Cosmochim. Acta*, *199*, 1-12.

de Koker, N., & Stixrude, L. (2009). Self-consistent thermodynamic description of silicate liquids, with application to shock melting of MgO periclase and MgSiO3 perovskite. *Geophys. J. Int.*, *178*, 162-179.

Di Paola, C. P., & Brodholt, J. P. (2016). Modeling the melting of multicomponent systems: the case of $MgSiO_3$ perovskite under lower mantle conditions. *Sci. Rep*, *6*. doi: 10.1038/srep29830

Du, Z., Jackson, C., Bennett, N., Driscoll, P., Deng, J., Lee, K. M., ... Fei, Y. (2017). Insufficient energy from MgO exsolution to power early geodynamo. *Geophys. Res. Lett.*, *44*. doi: doi.org/10.1002/2017GL075283

Du, Z., & Lee, K. M. (2014). High pressure melting of MgO from (Mg,Fe)O solid solutions. *Geoph. Res. Lett.*, *41*, doi:10.1002/2014GL061954.

Fiquet, G., Auzende, A. L., Siebert, J., Corgne, A., Bureau, H., Ozawa, H., & Garbarino, G. (2010). Melting of peridotite to 140 Gigapascals. *Science*, *329*, 1516-1518.

Fischer, R. A., & Campbell, A. J. (2010). High-pressure melting of wüstite. *Am. Mineral.*, *95*, 1473–1477.

Fischer, R. A., Nakajima, Y., Campbell, A. J., Frost, D. J., Harries, D., Langenhorst, F., ... Rubie, D. C. (2015). High pressure metal-silicate partitioning of Ni, Co, V, Cr, Si and O. *Geochim. Cosmochim. Acta*, *167*, 177-194.

Hirose, K., Morard, G., Sinmyo, R., Umemoto, K., Hernlund, J., Helffrich, G., & Labrosse, S. (2017). Crystallization of silicon dioxide and compositional evolution of the Earth's core. *Nature*, *543*, 99-102.

Huang, D., Badro, J., Brodholt, J., & Li, Y. (2019). Ab initio molecular dynamics investigation of molten FeSiO in Earth's core. *Geophys. Res. Lett.*, *46*, 6397-6405.

Jackson, C. R. M., Bennett, N. R., Du, Z., Cottrell, E., & Fei, Y. (2018). Early episodes of high-pressure core formation preserved in plume mantle. *Nature*, *553*, 491-495.

Kato, C., Hirose, K., Nomura, R., Ballmer, M., Miyake, A., & Ohishi, Y. (2016). Melting in the FeO-SiO_2 system to deep lower mantle pressures: Implications for subducted Banded Iron Formations. *Earth and Planet. Sci. Lett.*, *440*, 56-61.

Kimura, T., Ohfuji, H., Nishi, M., & Irifune, T. (2017). Melting temperatures of MgO under high pressure by micro-texture analysis. *Nature Comm.*, *8*, doi:10.1038/ncomms15735.

Liebske, C., & Frost, D. J. (2012). Melting phase relations in the MgO-$MgSiO_3$ system between 16 and 26 GPa: Implications for melting in the Earth's deep interior. *Earth and Planet. Sci. Lett.*, *345*, 159-170.

Mann, U., Frost, D. J., & Rubie, D. C. (2009). Evidence for high-pressure core-mantle differentiation from the metal-silicate partitioning of lithophile and weakly-siderophile elements. *Geochim. et Cosmochim. Acta*, *73*, 7360-7386.

Poirier, J.-P. (2000). *Introduction to the Physics of the Earth's Interior*. Cambridge, UK: Cambridge University Press.

Ricolleau, A., Fei, Y., Corgne, A., Siebert, J., & Badro, J. (2011). Oxygen and silicon contents of Earth's core from high pressure metalsilicate partitioning experiments. *Earth and Planet. Sci. Lett.*, *310*, 409-421.

Shen, G., & Lazor, P. (1995). Measurement of melting temperatures of some minerals under lower mantle pressures. *J. Geophys. Res.*, *100*, 17699-17713.

Siebert, J., Badro, J., Antonangeli, D., & Ryerson, F. J. (2013). Terrestrial accretion under oxidizing conditions. *Science*, *339*, 1194-1197.

Sun, Y., Song, H., Zhang, F., Yang, L., Ye, Z., Mendelev, M. I., ... Ho, K. (2018). Overcoming the time limitation in molecular dynamics simulation of crystal nucleation: a persistent-embryo approach. *Phys. Rev. Lett.*, *120*, 085703.

Wade, J., & Wood, B. J. (2005). Core formation and the oxidation state of the Earth. *Earth Planet. Sci. Lett.*, *236*, 78-95.

Table S1.

Table S1. Mg solubility model parameters

	a	σ_a	b	σ_b	c	σ_c	Source
				K	K/GPa		
K_D^{Si}	1.3	0.3	−13500	900			Fischer et al. (2015)
K_D^{Mg}	0.52	0.28	−10190	1059	−17.39	6.89	this study
K_D^{O}					−26.50	2.94	this study

$i-j$	MgO-SiO_2/kJ	σ/kJ	FeO-SiO_2/kJ	σ/kJ	
W_{i-j}	–		–		this study

$\varepsilon_i^j = \varepsilon_j^i$	$i \rightarrow$ / $j \downarrow$	Mg	$\sigma_{\varepsilon_j^{Mg}}$	Si	$\sigma_{\varepsilon_j^{Si}}$	O	$\sigma_{\varepsilon_j^{O}}$	ε_j^{Mg} source
	O	–	–	7.73	4.53	−9.16	4.27	this study
	Si	11.07	3.37	–	–			this study
	Mg	–	–					this study

–: not resolvable from data. O-O and O-Si interaction coefficients from Hirose et al. (2017).

Table S2.

Table S2: Ternary MgO-FeO-SiO_2 model parameters

Property	SiO_2(s)	SiO_2(l)	FeO(s)	FeO(l)	MgO(s)	MgO(l)	$MgSiO_3$(s)
F^0, G^0(kJ)	−819	−1469.3	−165	−787.397	−569	−809.361	−1568.175
S^0 (J/K)		275		578.242		173.5	
K^0 (GPa)				30.961			
V_0 (cc/mol)				18.776			
a_0 (/K)/10^{-5}				9.54849			
C_0 (J/K)				73.753[a]			
C_1 (J/K^2)/10^{-3}				3.0[a]			

Other values as reported in Boukaré et al. (2015). [a]Pers. comm. C.-E. Boukaré, 2018.

Table S3.

Table S3. Full EPMA analyses of coexisting liquid metal and silicate melt in ELSI runs reported by Badro et al. (2018).

Run#	002–43R	001–43	003–43	005–43	003–42	007–47	006–43
P (GPa)	30(3)	65(7)	108(11)	34(3)	89(9)	138(14)	59(6)
T (K)	3680(290)	5040(610)	4600(380)	3850(540)	4340(390)	5230(320)	5450(400)
Liquid metal (wt%)							
Fe	94.83(163)	85.57(57)	86.25(232)	90.23(76)	92.37(132)	77.99(212)	74.3(265)
Si	0.23(3)	2.05(22)	2.94(26)	1.83(15)	1.51(4)	8.68(41)	5.69(33)
O	3.19(16)	7.81(27)	5.05(38)	6.55(18)	3.05(11)	8.42(48)	8.02(124)
Mg	0.07(2)	0.54(7)	0.55(6)	0.23(4)	0.28(3)	0.77(9)	1.95(34)
Al	$< DL$	0.10(2)	0.11(3)	$< DL$	$< DL$	0.20(1)	0.30(9)
Ca	$< DL$	$< DL$	$< DL$	$< DL$	$< DL$	0.09(3)	0.12(2)
Na	$< DL$	$< DL$	$< DL$	$< DL$	$< DL$	$< DL$	$< DL$
K	0.24(5)	0.17(4)	0.31(8)	0.06(4)	0.09(3)	0.11(3)	0.30(5)
S	3.02(8)	2.88(6)	2.48(6)				
sum	101.68(197)	99.12(125)	97.69(319)	98.90(117)	97.30(153)	96.26(317)	90.68(472)
Silicate melt (wt%)							
SiO_2	42.83(38)	36.09(96)	34.16(137)	34.50(32)	39.31(162)	35.32(66)	35.46(35)
MgO	21.37(35)	26.28(103)	28.01(118)	21.93(59)	25.38(304)	26.4(61)	35.33(50)
FeO	14.56(73)	16.15(171)	17.61(138)	30.79(67)	20.12(328)	20.67(182)	14.72(137)
Al_2O_3	2.81(6)	5.88(20)	6.31(35)	2.39(57)	6.14(25)	6.79(18)	5.96(12)
CaO	3.67(18)	2.70(12)	1.85(5)	2.45(12)	1.48(13)	2.62(16)	3.04(8)
Na_2O	0.88(7)	0.29(4)	0.39(4)	0.93(4)	0.33(8)	0.41(3)	0.68(2)
K_2O	9.36(18)	8.45(20)	9.22(61)	9.94(15)	4.36(13)	2.37(6)	6.20(15)
SO_3	$< DL$	0.32(30)	0.32(10)				
sum	95.48(195)	96.16(456)	97.87(508)	102.93(246)	97.12(853)	94.58(352)	101.39(259)

Parentheses indicate uncertainty in final digits. $< DL$: less than detection limit.

Figure S1.

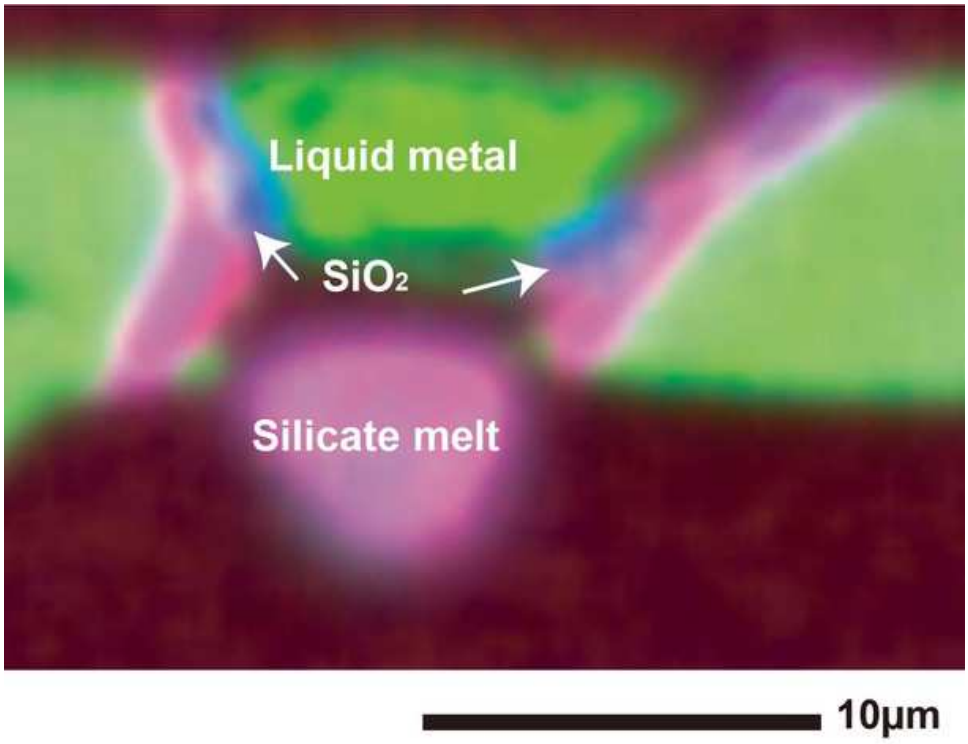

Supplementary Figure S1. Melting experiment in a laser-heated DAC on a homogeneous Fe-7.21%Si-13.84%O-1.43%Mg (in weight) sample in KCl pressure medium at 25(3) GPa and 3200(320) K. X-ray chemical map (combining individual X-ray images for Fe, Si, and Mg) of a cross section of the recovered sample shows quenched metal liquid (darker green) and silicate melt (pink) at the center (the hottest part), surrounded by solid SiO_2 (blue), Mg-silicate (pink) and unmelted starting material (lighter green). The starting material was produced by sputtering of Fe, Si, and Mg atoms on a glass slide under O_2 flow. Other experimental procedures were similar to those in Hirose et al. (2017).

Figure S2.

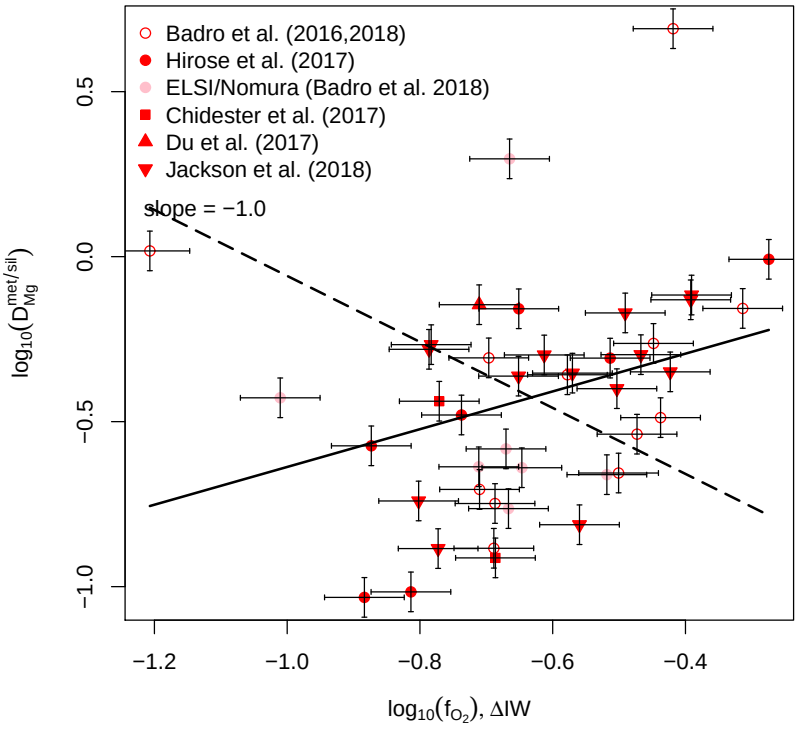

Supplementary Figure S2. D_{Mg} dependence on f_{O_2} defined by the Fe-FeO (IW) buffer. All available data obtained by previous laser-heated DAC experiments are used (Badro et al., 2016; Chidester et al., 2017; Du et al., 2017; Jackson et al., 2018). While the slope of -1.0 (dashed line) is expected for the exchange reaction Fe + MgO = Mg + FeO, the data are scattered and the best estimated slope (solid line) has a positive slope, indicating limitations on exchange of O between the metal, silicate and experimental environment. We therefore made an alternative approach considering the exchange reaction Si + 2MgO = 2Mg + SiO_2 (see Figure S3).

Figure S3.

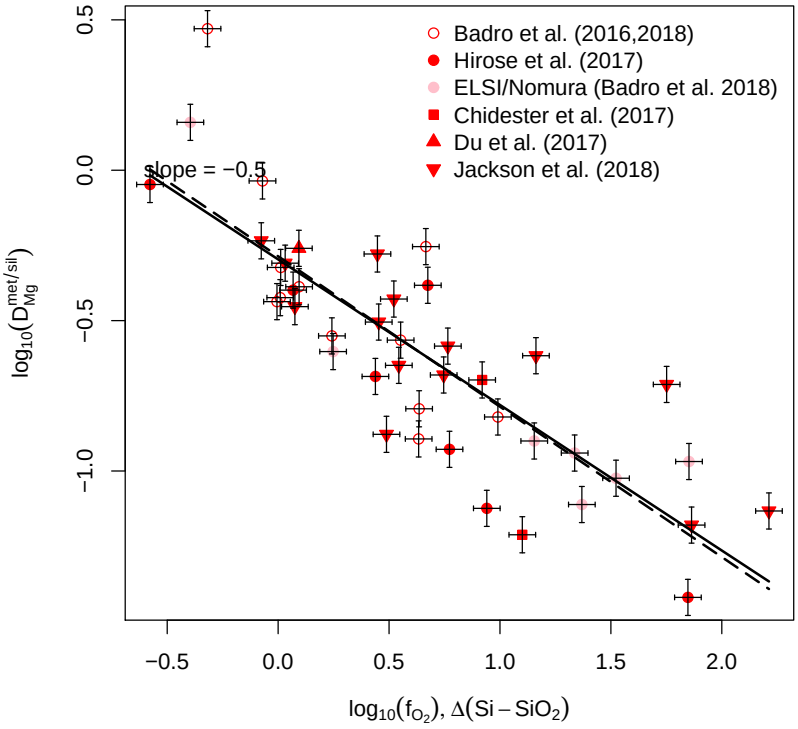

Supplementary Figure S3. D_{Mg} dependence on f_{O_2} defined by the Si-SiO_2 buffer. Same data set was used as Figure S2. The slope (solid line) of $\log_{10} D_{Mg}$ vs. f_{O_2} is controlled by the +2 valence of Mg. A slope of $\frac{1}{2}$ (dashed line) is expected for a two valence unit exchange reaction, showing that the present thermodynamic modelling approach considering the exchange reaction Si + 2MgO = 2Mg + SiO_2 is valid.

Figure S4.

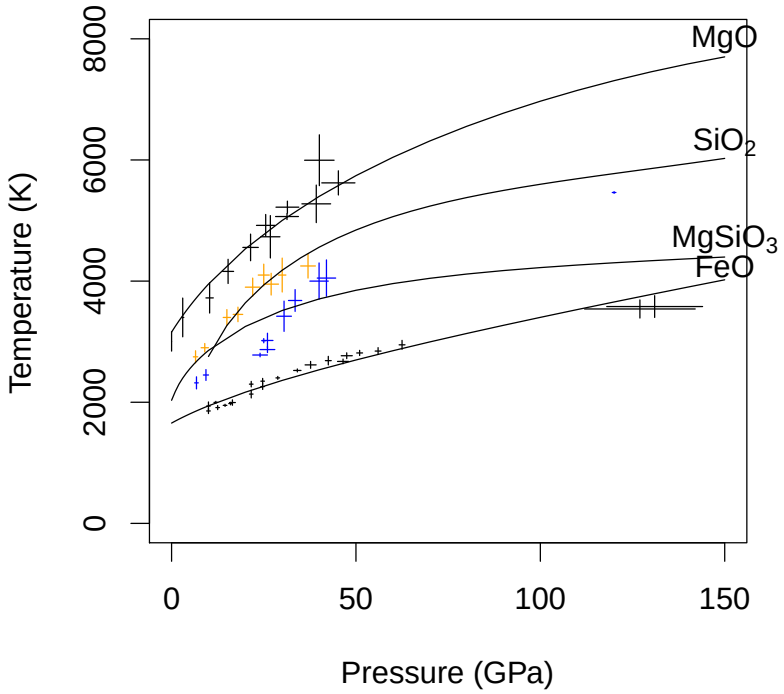

Supplementary Figure S4. Fits of melting curve data based on the revised liquid equations of state for endmembers, MgO, FeO and SiO_2. Data points are from Shen and Lazor (1995) for SiO_2, Shen and Lazor (1995), de Koker and Stixrude (2009), Liebske and Frost (2012) and Di Paola and Brodholt (2016) for $MgSiO_3$, Du and Lee (2014) and Kimura, Ohfuji, Nishi, and Irifune (2017) for MgO, and Fischer and Campbell (2010) and Kato et al. (2016) for FeO.

Figure S5.

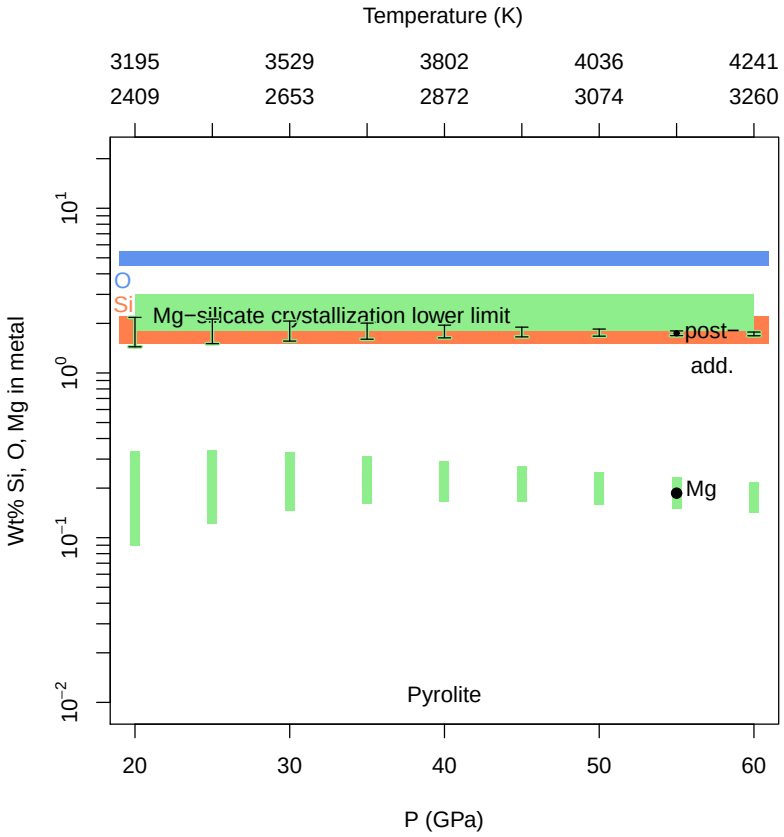

Supplementary Figure S5. Saturation of Mg in core metal in a single-stage core formation scenario. Concentration of Mg in metal in equilibrium with silicate in a single-stage core formation scenario at different magma ocean pressures. Top axis labels give temperature range of solidus (low) and liquidus (high) temperatures at each core formation pressure (Fiquet et al., 2010). Error bars on lower Mg range indicate uncertainty due to choice of solidus or liquidus conditions, estimated from the MgO solubility in metal using K_D expressions (Table S1). No feasible magma ocean depth yields levels required for Mg-silicate or MgO exsolution from the core ($> 1.7 \pm 0.5$ wt% Mg in the metal). Added Mg from late metal addition event (upper uncertainty band) uses minimum 1.7 wt% Mg concentration. For comparison, O and Si bands from Siebert, Badro, Antonangeli, and Ryerson (2013).